31st Annual International Conference of the IEEE EMBS
Minneapolis, Minnesota, USA, September 2-6, 2009

Fluorescence Molecular Tomography with Optimal Radon Transform Based Surface Reconstruction

Xin Liu, Daifa Wang, and Jing Bai*, *Fellow, IEEE*

***Abstract*—Full angle non-contact fluorescence molecular tomography allows acquiring large data sets from complete angles, and simplifies the experimental setups. Accurately extracting animal surface is important for this kind of imaging systems. However, in in-vivo experiments, mouse breath movements and mechanical errors will influence the surface reconstruction. An optimal radon transform based surface reconstruction method is proposed to handle these two factors. The proposed method uses a line searching method to minimize the mismatch between the reconstructed 3D surface and the projected silhouettes at different angles. Therefore, the proposed method generates the optimal 3D surface compared to other methods based on radon transform. Results show that the mean mismatch of 3D surface generated is less than two CCD pixels (0.154 mm) in in-vivo experiments. In-vivo fluorescence molecular tomography is also performed to demonstrate the efficiency of the proposed method.**

I. Introduction

FLUORESCENCE molecular tomography (FMT) is an emerging diagnosis tool for small animal research and drug discovery. By tagging regions of interest with target specific fluorescence molecular probes, fluorescence molecular tomography may resolve three dimensional (3D) locations and geometries of target areas, such as tumors [1, 2]. At present, this new technology has been widely used for gene function, proteins, enzymes, metastasis, drug discovery, and cancer detection in vivo combined an increasing number of fluorescent probe technologies [1-4].

To date, fluorescence tomography systems have evolved from the early fiber-based systems [5] to the non-contact slab-shaped system using charge coupled device (CCD) [6]. However, the above systems require fixed geometries and matching fluids, which are inconvenient for experiments. FMT with complete angle projections overcomes the limited projection angles of the fixed geometry, which gets more accurate localization and quantification information of fluorescent [7, 8]. Additionally, it gets rid of matching fluids, which simplifies the experimental setups [7, 8].

Manuscript received April 22, 2009. *Asterisk indicates corresponding author.*

This work was supported by the National Nature Science Foundation of China (No. 30670577, 60831003), the Tsinghua-Yue-Yuen Medical Science Foundation, the National Basic Research Program of China (No. 2006CB705700), the National High-Tech Research and Development Program of China (No. 2006AA020803), and the China Postdoctoral Science Foundation Funded Project.

Xin Liu, Daifa Wang, and Jing Bai are with the Department of Biomedical Engineering, School of Medicine, Tsinghua University, Beijing, 100084, China (e-mail: deabj@mail.tsinghua.edu.cn).

Accurate knowledge of the mouse surface is very important for FMT reconstruction. With this information, the light transportation in the mouse can be predicted using diffusion equation (DE) [7-10]. In [10], the mouse surface is obtained using a photogrammetric 3D camera. Structured light is also used for obtaining the mouse surface in Xenogen IVIS Imaging system 200 Series [11]. In full angle non-contact imaging systems [7, 8, 12], the mouse surface can be reconstructed from white light [13, 14] or shadow images [7] captured at different angles. This technique takes full advantage of the full angle non-contact imaging system. Thus, no extra equipment is needed.

Radon transform with constant filter [7] or Sheep Logan filter [14] has been used for reconstructing the mouse surface. In this paper, we point out the essential of randon transform based surface reconstruction methods. Reconstructing a 2D outline using randon transform from projection lines is to find one polygon of the real 2D geometry. This finding determines the theoretical optimal parameter for extracting the 2D outline from the back projected 2D image. In practical in-vivo experiments, the optimal parameter will be different from the theoretical one as the result of mouse movements and mechanical errors. A line searching method is introduced to obtain an optimal parameter which minimizes the mismatch between the reconstructed 2D outline and the projected lines.

To reconstruct the optimal 3D surface, we first extract the silhouette binary images from the white light projections based on sobel operator and active contour method for each angles [15, 16]. Then, at each slice, the radon transform with constant filter is performed. After that, a line searching method is used to find the optimal 2D geometry from the projected 2D image at each slice.

This paper is organized as follows. Section 2 mainly presents the experimental setups and methods. In-vivo FMT results are reported in Section 3 and conclusions are made in Section 4.

II. Methods

A. Experimental setups

To implement complete angle projection FMT, a free-space system was generated [12], as shown in Fig. 1. The mouse was suspended on a rotating stage. The system allowed rotation and shift of the target around its z axis for collecting complete angle projections. An isoflurane vaporizer was used to anesthetize the mouse during the in-vivo measurements.

The small light spot from a 250 W Halogen lamp traveled through a 775 nm band pass filter to provide the excitation light. Data were recorded by a 512x512 pixel, -70°C cooled EMCCD array coupled with a Nikkor 60 mm f/2.8D lens.

When collecting fluorescence images, a 840 nm band-pass filter was used. When collecting the excitation light images, a neutral density filter of 6% transmittance was used. When collecting the white light images, a white light bulb was used to replace the excitation light and the neutral density filter was still used.

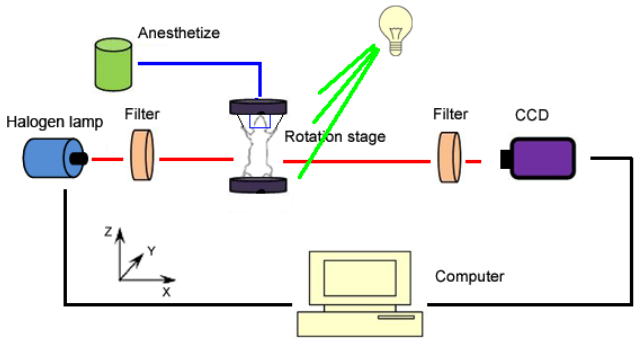

Fig.1. Experimental setup

White light images, excitation images and fluorescence images were acquired in the same geometry and identical placement conditions. For 3D surface reconstruction, 72 projections were collected with an increment of 5 degree. For the acquisition of the fluorescence and excitation images, 36 projections were collected every 10 degree.

B. Edge detection method

Before reconstructing 3D surface, it is important to accurately extract the silhouette information from the captured projections.

First, based on the characteristics of the projections, we obtain the initial segmentation results using vertical gradient operator. Herein, we specify the sensitivity threshold value for sobel algorithm, which is used to further threshold the calculated gradient magnitude. Second, based on the sobel segmentation results, we acquire more accurate edge information using active contour methods. Considering the time factors, 20 iterations are performed for each projection.

C. Surface reconstruction method

With extracted silhouette at different angles in section 2.B, the 3D surface is obtained by reconstructing 2D outlines at each height slice. At each slice, the 2D outline information is obtained by back projecting all the projection lines of the objects at this height, equivalent to the radon transform method with a constant filter [13].

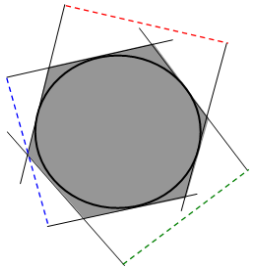

Fig.2. Essential of randon transform based surface reconstruction methods. The dashed lines are projection lines collected. The gray region formed by back projection is a circumscribing polygon of the real 2D geometry.

Fig.2. illustrates the essential of radon transform based surface reconstruction methods. Reconstructing the 2D outline from projected lines is to find one circumscribing polygon of the real 2D geometry. As the increase of projection angles, the circumscribing polygon will approximate the real 2D geometry accurately. Theoretically, once the region occupied by the object is obtained, the most accurate 2D geometry can be extracted by finding the unity pixels. The unity pixel is the pixel has the maximum gray value and appears in all projections. Finding unity pixels means finding pixels using threshold 1. However, in in-vivo experiments, the theoretically determined threshold doesn't produce the most approximate 2D geometry as the result of mouse breath movements and mechanical errors. For example, [7] said good results were consistently generated with threshold set to 0.8.

It should be noted that the mouse breath movements in different regions are different. For example, the mouse breath movements in chest region are larger than in abdomen region. At the same time, the mechanical errors of different FMT systems will be slightly different. An optimal threshold at each slice j is determined using the following formula:

$$th_j = \min\{\sum_{\theta_i}[abs(L(j,\theta_i)_{left} - \vec{L}_{th}(j,\theta_i)_{left}) + abs(L(j,\theta_i)_{right} - \vec{L}_{th}(j,\theta_i)_{right}]\}, \quad (1)$$

where $L(j,\theta_i)$ is the collected projection line at angle θ_i, and $\vec{L}_{th}(j,\theta_i)$ is the projection line at angle θ_i of reconstructed 2D geomtry with threshold set to th. Subscript *left* and *right* are the left and right position of projection lines. Eq. (1) finds the optimal threshold th_j by minimizing the mismatch between the reconstructed 2D geometry and collected silhouette at different angles. Because Eq. (1) is a unimodal function, one dimensional line searching method can be used to find the optimized threshold. In this paper, the golden section method is employed to search the optimal threshold during the region from 0.8 to 1.0.

D. Finite element based FMT reconstruction method

For in-vivo FMT reconstruction, the normalized born

method [6] is used for reconstruction. A linear system $m = Wn$ is generated based on the diffusion equation [9]. For reconstruction, Random access algebraic reconstruction technique (R-ART) is employed to solve the linear system.

III. RESULTS

A. Segmentation results

As a comparison, the edge detection algorithm based soble operator and active contour method was applied to segment 72 projections every 5 degree. The segmentation results are shown in Fig. 3, where we present the original data, the initial segmentation result based on sobel operator, and final segmentation result based on contour method, respectively, for a single projection.

(a) (b) (c)

Fig.3. Segmentation results for a single projection. (a) is white light projection data, (b) is binary segmentation result for edge detection algorithm based on soble operator, and (c) displays the final segmentation result based on contour method that the outline of segmentation image place the original data.

B. Surface reconstruction results

As shown in Fig. 4(a) and (b), the reconstructed 3D surface with optimal threshold is mapped to the projected white light images at 0 and 55 degrees respectively. In contrast, the reconstructed 3D surface with a constant threshold 0.7 [7] is also mapped to the projected white light images, as shown in Fig. 4(d) and (e). It is obvious that the optimal threshold matches the projected white light images much better than a constant threshold 0.8. Fig. 4(f) shows the mean mismatch between the extracted 2D outline with different threshold and the projection lines.

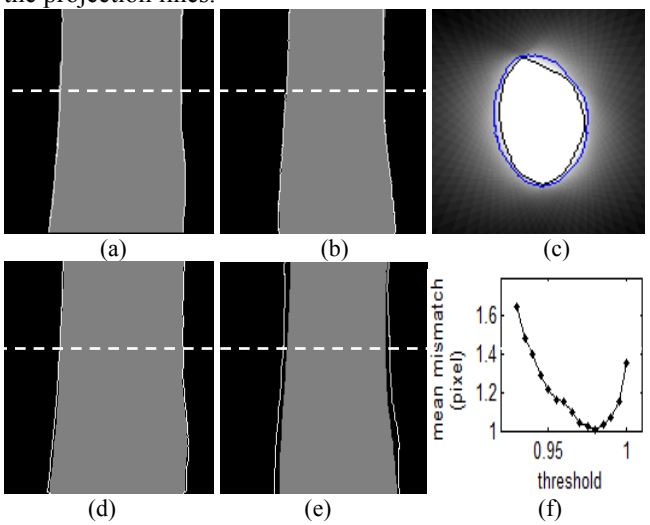

(a) (b) (c) (d) (e) (f)

Fig.4. Surface reconstruction results. The extracted 3D surface with the optimal threshold is mapped to projection images respectively, (a) 0 degree, (b) 55 degree. The extracted 3D surface with threshold 0.8 is mapped to projection images respectively, (d) 0 degree, (e) 55 degree. White lines in (a), (b), (d), and (e) are corresponding to the 3D surfaces, while the gray region indicate the collected silhouette. Dashed lines in the (a), (b), (d) and (d) indicate the 2D slice used in (c) and (f). (c) is the result based on randon transformation, in which black line represents extracted 2D outline with the optimal threshold parameters, while the blue line represents that with the constant threshold 0.8 [7]. (f) is the mean mismatch between the extracted 2D outline with different thresholds and projection lines.

The reconstructed 3D surface result between lower bottom abdomen and middle chest is shown in Fig.5 using 72 projections with an increment of 5 degree. For each projection, expose time is 0.7 s.

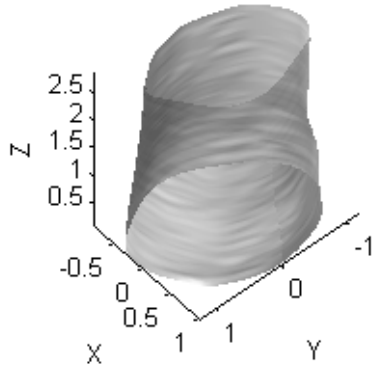

Fig.5. The reconstructed 3D surface with the optimal threshold parameter. The axis unit is cm.

C. Fluorescence tomography results

To demonstrate the ability of the method to resolve fluorescence target distribution, one transparent glass tube was implanted into the mouse subcutaneously. The diameter of the tube was 1 mm and it was filled with 7 mm length ICG of 10 uM concentration. The weight matrix was generated on a finite element mesh with 372 triangle elements and 217 nodes. 50 R-ART iterations were performed with relaxation parameter set to 0.1.

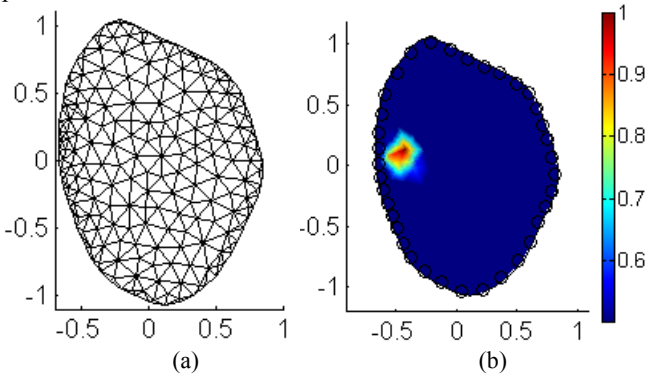

(a) (b)

Fig.6. Reconstructed FMT result using 36 projections obtained from an anesthetic mouse implanted with one fluorescent tube. (a) the finite element mesh used. (b) Reconstructed image normalized to its maximum value. Two band-pass filters are used: 775nm for the excitation source and 840 nm for ICG emission. The axis unit is cm.

IV. CONCLUSION

In this paper, an optimal threshold determination method

was proposed to generate the most accurate 3D surface from the projected white light images. A sobel vertical-gradient method was also proposed to efficiently extract the silhouette from the projected white light images. Results demonstrated that the method proposed generated the most accurate 3D surface with mismatch less than 2 CCD pixels (0.154 mm) in in-vivo experiments. With the 3D surface, FMT tomography results were also provided.

Future studies will be focused on applying the proposed method to research in cancer and drug delivery.

REFERENCES

[1] R. Weissleder and M.J. Pittet, "Imaging in the era of molecular oncology," nature, vol. 42, pp. 580-589, Apr. 2008.

[2] R. Weissleder, "Molecular Imaging in Cancer," Science, vol. 312, pp. 1168-1171, May. 2006.

[3] V. Ntziachristos, J. Ripoll, and R. Weissleder, "Looking and listening to light: The evolution of whole-body photonic imaging," Nat. Biotechnol., vol. 23, no. 3, pp. 313-320, Mar. 2005.

[4] Z.Z. Han, A. Fu, and D.E. Hallahan, "Noninvasive assessment of cancer response to therapy," Nat. Med., vol. 14, no. 3, pp. 343-349, Mar. 2008.

[5] J. Chang, H. L. Graber, and R. L. Barbour, "Luminescence optical tomography of dense scattering media," J. Opt. Soc. Am A vol. 14, no. 1, pp. 288-299, Jan. 1997.

[6] E. E. Graves, R. Weissleder and V. Ntziachristos, "A submillimeter resolution fluorescence molecular imaging system for small animal imaging," Med. Phys., vol. 30, no. 5, pp. 901-911, May. 2003.

[7] H. Meyer, A. Garofalakis, and J. Ripoll, "Noncontact optical imaging in mice with full angular coverage and automatic surface extraction," Appl. Opt., vol. 46, no. 17, pp. 3617-3627, June. 2007.

[8] N. Deliolanis, T. Lasser, and V. Ntziachristos, "Free-space fluorescence molecular tomography utilizing 360° geometry projections," Opt. Lett., vol. 32, no. 4, pp. 382-384, Feb. 2007.

[9] X. Song, D. Wang, and J. Bai, "Reconstruction for free-space fluorescence tomography using a novel hybrid adaptive finite element algorithm," Opt. Express, vol. 15, no. 26, pp. 18300-18317, Dec. 2007.

[10] R. B. Schulz, J. Ripoll, and V. Ntziachristos, "Experimental fluorescence tomography of tissues with noncontact measurements," IEEE Trans. Med. Imaging, vol. 23, no. 4, pp. 492–500, Apr. 2004.

[11] XENOGEN, U.S. patent application 20060268153, Nov. 2006.

[12] G. Hu, J. Yao, and J. Bai, "Full-angle optical imaging of near-infrared fluorescent probes implanted in small animals," Progress in Natural Science, vol. 19, pp. 707-711, 2008.

[13] T. Lasser, A. Soubret, and V. Ntziachristos, "Surface Reconstruction for Free-Space 360o Fluorescence Molecular Tomography and the Effects of Animal Motion," IEEE Trans. Med. Imag., vol. 27, no. 2, pp. 188-194, Feb. 2008.

[14] J. Yao, G. Hu, and J. Bai,"A 3D-surface Torso Reconstruction Method Used in Fluorescence Molecular Tomography of Small Animals," Chinese Journal of Biomedical Engineering, vol. 27, no.3 , pp. 360-365, June. 2008.

[15] J. Canny, "A Computational Approach to Edge Detection," IEEE Trans. Pattern Anal. Mach. Intell., vol. 8, no. 6, pp. 679-698, Nov. 1986.

[16] T.F. Chan, "Active Contours Without Edges," IEEE Trans. Image Processing, vol. 10, no. 2, pp. 266-277, Feb. 2001.